CANCER

Genomic mapping in outbred mice reveals overlap in genetic susceptibility for HZE ion– and γ-ray–induced tumors

E. F. Edmondson[1,2]*, D. M. Gatti[3], F. A. Ray[2], E. L. Garcia[2], C. M. Fallgren[2], D. A. Kamstock[2], M. M. Weil[2]*

Cancer risk from galactic cosmic radiation exposure is considered a potential "showstopper" for a manned mission to Mars. Calculating the actual risks confronted by spaceflight crews is complicated by our limited understanding of the carcinogenic effects of high-charge, high-energy (HZE) ions, a radiation type for which no human exposure data exist. Using a mouse model of genetic diversity, we find that the histotype spectrum of HZE ion–induced tumors is similar to the spectra of spontaneous and γ-ray–induced tumors and that the genomic loci controlling susceptibilities overlap between groups for some tumor types. Where it occurs, this overlap indicates shared tumorigenesis mechanisms regardless of the type of radiation exposure and supports the use of human epidemiological data from γ-ray exposures to predict cancer risks from galactic cosmic rays.

INTRODUCTION

Interplanetary space is populated by densely ionizing particle radiation not naturally present on Earth (*1*). Life on Earth has evolved under the protection of a geomagnetic field, which deflects high-charge, high-energy (HZE) ions; however, the constant flux of HZE ions in deep space is essentially impossible to shield, making astronaut exposures inevitable (*2*).

In the absence of human epidemiological data for exposures to HZE radiation, uncertainties surround the cancer risk estimates for space flight crews that venture beyond low Earth orbit. The current NASA space radiation cancer risk model is built largely upon epidemiological data from the survivors of the Hiroshima and Nagasaki atomic bombings, a cohort of individuals exposed predominantly to γ-rays (*3*–*5*), a form of photon radiation. One key assumption in this NASA model is that the spectra of tumor types, and their biologic behaviors, will be similar for individuals exposed to ionizing radiation, whether particle or photon. However, notable physical differences exist between ionizing photon and particle radiation, and these physical differences translate to unique ionization and damage patterns at the molecular, cellular, and tissue levels. HZE ion exposures produce spatially clustered DNA double-strand breaks, along with other DNA lesions in close proximity to break sites (*6*). In contrast, γ-rays produce sparse ionization events that are random in spatial distribution and less likely to have additional DNA lesions immediately adjacent to the break sites. Other assumptions in the model are that radiogenic tumors are no more lethal than their sporadic counterparts and that females are at greater risk for radiogenic cancers than males (*7*).

In assessing cancer risks to astronauts, the premise that HZE ion exposures increase the risk for the same types of tumors that arise in human populations exposed to γ-rays is supported by the few animal studies of HZE ion carcinogenesis conducted to date (*8*). These studies, conducted on genetically homogeneous animals, have demonstrated that tumor types arising in HZE ion–irradiated animals are the same as those that occur spontaneously in these animals or following exposure to photon radiation (*8*). However, all previous data are from either inbred mice (*9*, *10*) or rats (*11*), F1 hybrid mice (*12*, *13*), or rat stocks with limited genetic heterogeneity (*11*, *14*–*16*), and the tumor types that arise in inbred rodents are determined, in very large part, by their genetic background. Therefore, the spectrum of tumors that might arise in a genetically diverse population exposed to HZE ions is unknown.

With the emergence of multiparent outbreeding strategies that produce highly recombinant mouse populations with allelic variants from multiple founder strains (*17*–*19*), it is possible to model the effects of population diversity in carcinogenesis studies by minimizing the overwhelming effects of genetic background and increasing the phenotypic repertoire available within a test population. These populations also allow for high-precision genetic mapping (*18*, *20*). Quantitative trait locus (QTL) mapping is a powerful forward-genetics approach that allows for unbiased testing of genetic variants that may influence gene-environment interactions for radiation effects (*21*, *22*). Highly recombinant populations were constructed for the purpose of mapping complex traits, and QTL can often be resolved to megabase resolution (*18*–*20*). In addition, complete sequence information can be used on genotyped individuals by imputing the substantial genomic resources available for the founder strains.

Studying tumors that arise in irradiated, genetically diverse mouse populations presents a unique opportunity to test key assumptions of the NASA risk model, particularly whether HZE ions induce the same tumors by the same mechanisms as γ-rays. If so, the current practice of extrapolating human epidemiological data from individuals exposed to γ-rays to astronauts exposed to HZE ions would be a valid approach for risk calculation in the space radiation environment.

RESULTS

Characterizing the tumor spectrum in HZE ion–irradiated outbred mice

To study the effects of HZE ion irradiation in a genetically heterogeneous population, 1850 HS/Npt stock mice (*23*) of both sexes

[1]Frederick National Laboratory for Cancer Research, Frederick, MD 21702, USA. [2]Colorado State University, Fort Collins, CO 80523, USA. [3]The Jackson Laboratory, Bar Harbor, ME 04609, USA.
*Corresponding author. Email: michael.weil@colostate.edu (M.M.W.); elijah.edmondson@nih.gov (E.F.E.)

were genotyped for 77,808 single-nucleotide polymorphism (SNPs) and exposed to (i) 0.4 gray (Gy) of ^{28}Si ions (240 MeV/n) [linear energy transfer (LET), 80 keV/μm; Φ = 0.031 particles/μm^2] or (ii) ^{56}Fe ions (600 MeV/n) (LET, 181 keV/μm; Φ = 0.014 particles/μm^2), (iii) 3 Gy of ^{137}Cs γ-rays, or (iv) sham irradiation. We chose ^{56}Fe ions because of their high abundance in galactic cosmic radiation (GCR) and because their high charge (Z = +26) makes them particularly damaging (*24*). The ^{28}Si ions were selected because their LET more closely approximates the dose average LET of secondary fragments generated by GCR penetrating an aluminum spacecraft hull (*25*). The mice were monitored daily until they reached 800 days of age or became moribund. Comprehensive necropsies were performed on each mouse and involved all organ systems. Each detected lesion was characterized histologically by a board-certified veterinary pathologist. Tumors were the predominant cause of morbidity and mortality for both HZE ion–irradiated (n = 622) and γ-ray–irradiated (n = 615) populations as well as for the population of unirradiated mice (n = 613). Overall life span was significantly reduced for irradiated populations (Fig. 1A), which can be attributed to the increased incidence and decreased median survival for radiation-induced tumors. For irradiated mice, populations exposed to 0.4-Gy HZE ions had increased survival times compared to mice exposed to 3.0 Gy of γ-rays (Fig. 1A). Although these doses seem disparate, their selection is based on preliminary dose-response studies (*26*), which reveal that 0.4 Gy of HZE ions and 3.0-Gy γ-rays are each maximally tumorigenic.

A wide variety of tumor diagnoses [82 distinct tumor histotypes (table S1)] were observed in HS/Npt mice. Although most of these tumor types were rare, 18 histotypes were observed at incidences greater than 1%. Overall, the spectra of tumor histotypes produced in genetically diverse populations exposed to HZE ions and γ-rays were similar (Fig. 1B). Furthermore, tumor types induced by radiation were generally similar to those arising spontaneously in HS/Npt mice; however, radiation-exposed populations demonstrated decreased median survival times associated with tumor development (Fig. 1C and figs. S7 to S22) and increased incidences for specific tumor types, such as leukemias and Harderian gland adenocarcinomas, following radiation (Fig. 1B). The structure of the HS/Npt population can be divided into families that consist of mice more closely related to one another. Many tumor histotypes show high incidences within some families but are absent or rare in others (Fig. 1, D to F), which is consistent with genetic susceptibility to certain tumor types. Furthermore, certain tumors—particularly lymphomas, pulmonary adenocarcinomas, hepatocellular carcinomas, Harderian gland tumors, and myeloid leukemias—demonstrate a periodicity in tumor incidence (Fig. 1, D to F) where adjacent families often display similar incidences, which could be predicted on the basis of the circular breeding design used to generate HS/Npt, in which adjacent families are more related to one another than families further removed.

Although the tumor spectra are similar for each irradiated population, the different radiation qualities demonstrate varied efficiencies for producing specific tumor histotypes. γ-ray–irradiated mice were at greater risk for myeloid leukemia, T cell lymphoma, pituitary tumors, and ovarian granulosa cell tumors than unirradiated mice; HZE ion–irradiated mice demonstrated an intermediate susceptibility to these histotypes (Fig. 1B). For Harderian gland tumors, thyroid tumors, hepatocellular carcinomas, and sarcomas, HZE ion– and γ-ray–irradiated mice were at a similarly and significantly increased risk compared to unirradiated controls (fig. S7 to S22).

NASA permissible exposure limits for radiation limit the number of days an astronaut can spend in space based on modeled cancer risk. These limits are different for men and women (*27*) due primarily to epidemiological data that indicate that women are at greater risk for radiogenic cancers than men due to their longer life spans and susceptibility to specific cancer types, such as lung, ovarian, and breast carcinomas. Female HS/Npt mice have longer life spans than males ($P = 2.7 \times 10^{-6}$, log-rank test), with unirradiated females living 43 days longer (686.1 days), on average, than males (643.2 days) (fig. S1A). In contrast, no survival difference is observed between γ-ray–irradiated females and males (P = 0.51) or HZE ion–irradiated females and males (P = 0.06), indicating that female HS/Npt mice are more susceptible to radiation-induced morbidities and mortalities than males (fig. S1, B and C). Irradiated female mice had increased incidences of (i) ovarian tumors, (ii) mammary tumors, (iii) central nervous system tumors (pituitary adenomas, choroid plexus tumors, and ependymomas), (iv) diffuse large B cell and lymphoblastic B cell lymphomas, (v) osteosarcomas, and (vi) leiomyosarcomas (fig. S1D). Female mice were at lower risk for radiogenic lung cancer (fig. S1D and table S1), which is a major contributor to limiting flight time for female astronauts. Modeling risk by sex in humans has been confounded by different smoking rates between men and women in the atomic bomb survivor cohort (*28*).

QTL mapping

To determine whether the genetic variants that increase tumor susceptibility following γ-ray irradiation also increase tumor susceptibility following HZE ion irradiation, genome-wide association mapping was performed for 18 tumor types in which there was an incidence of greater than 1%. Genomes were reconstructed for each mouse using a probabilistic model to predict founder haplotypes from high-density genotype data (*18*). Reconstructed genomes represent the unique accumulation of meiotic events for each individual and form a scaffold for the imputation of known sequencing information from the eight parental inbred strains. Polygenic covariance among related individuals is of significant concern in multiparent crosses and was corrected for during QTL mapping with a kinship term (*18*, *29*). Mapping was performed for each phenotype using both a generalized linear mixed-effects model and proportional hazards regression model with the aforementioned kinship to adjust for polygenic covariance between related mice. To determine the significance thresholds for a model in which no QTL is present, the phenotypes were permuted, the regression model was run, and the maximum statistic was retained from each permutation (*30*). The 95% significance threshold was minimally variable between phenotypes with a mean threshold of $-\log(P) > 5.8$, and this value was used to identify significant associations. This is consistent with the estimated 0.05 Bonferroni genome-wide corrected threshold of $-\log(P) > 6.0$, which is considered overly conservative for QTL mapping (*30*).

At least one QTL was identified for 13 of the 18 tumor phenotypes examined. For tumor incidence, 35 QTL were identified with an average confidence interval of 3.4 Mb (table S2). For QTL at the 95% confidence threshold, effect sizes average 3.7% of the phenotypic variance with a range of 0.75 to 7.46%. For most of the tumors, the genetic architecture was complex with multiple QTL individually explaining a small proportion of the total variance. Although

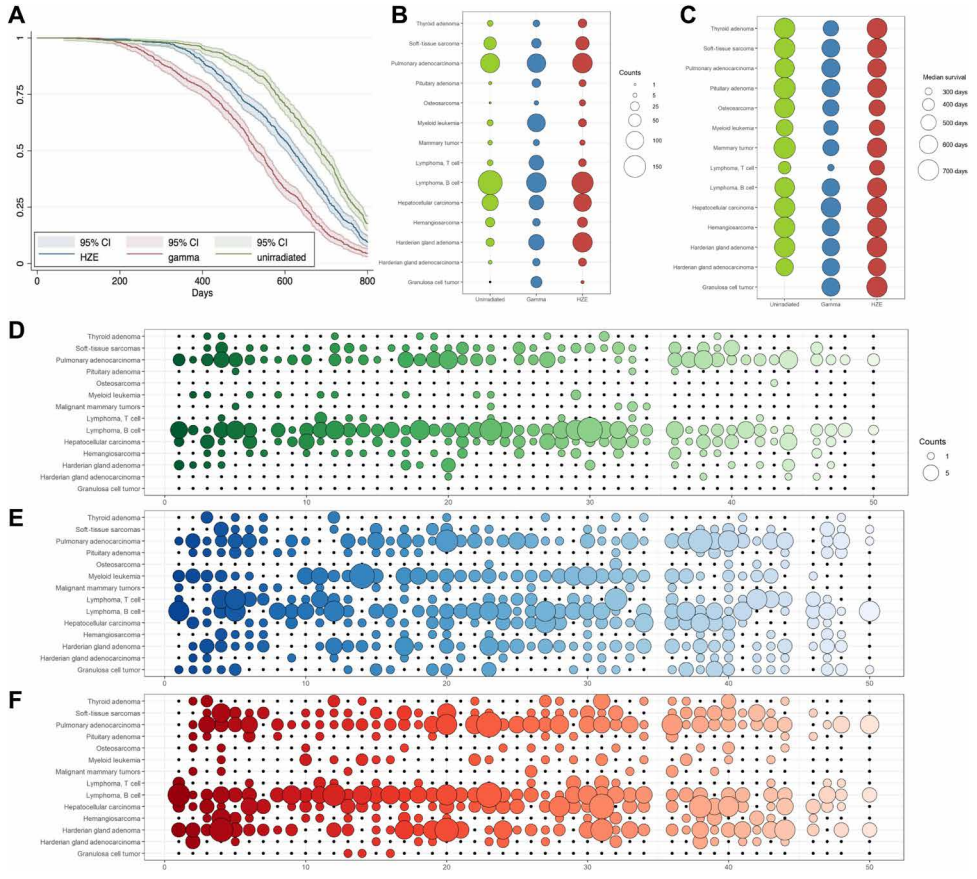

Fig. 1. Comparison of HZE ion and γ-ray exposures on survival and tumor incidence in genetically diverse mouse populations. Overall survival for HS/Npt mice, plotted as Kaplan-Meier survival, is presented for each exposure group (**A**). The incidence of specific tumor histotypes (**B**) and median survival times for these tumors (**C**) are plotted for each exposure group, which demonstrates that certain tumor types occur at an increased frequency following exposures to radiation of specific qualities and survival times in irradiated mice are decreased for some tumor types. The incidence of specific tumor histotypes within HS/Npt families is plotted for unirradiated (**D**), γ-ray–irradiated (**E**), and HZE ion–irradiated families (**F**) and demonstrates that specific tumor types often occur at very high incidence within some families and not at all in others, indicating heritability of tumor susceptibility. Furthermore, adjacent families are more closely related, and tumor incidences, for example, family 23 and adjacent families, have a high incidence of B cell lymphoma. The 47 HS/Npt families are arranged along the *x* axis (D to F).

loci with moderate effects on the phenotype were most common, 11 large effect QTL were observed for seven tumor histotypes, with effect sizes greater than 5% (table S2).

To determine potential effects of genetic variants on tumor latency following irradiation, mapping was also performed using proportional hazards regression model (table S3) and 38 QTL were identified for 12 tumor types. QTL associated with tumor survival times mirrored those identified for tumor incidence, indicating that the genetic variants that control susceptibility to radiation-induced tumors also determine latencies.

Neoplasia is a binomially distributed trait, and therefore, the power to detect significant associations is primarily dependent on tumor incidence and QTL effect size. This leads to important considerations for the ultimate goal of this analysis, which is to determine similarities between QTL for specific neoplasms in populations exposed to different qualities of radiation. For some tumor types, a significant peak was observed in one exposure group with a suggestive peak present at the same locus in the alternative exposure group. We speculate that the reason certain radiation qualities produce only suggestive QTL for certain tumor phenotypes is likely due to decreased mapping power as a result of the variation in incidence between groups. In these cases, if the peak was more significant when combining radiation groups, the QTL was considered significant for all irradiated animals regardless of radiation quality.

Comparing QTLs: Thyroid tumors following HZE ion and γ-ray exposures

Thyroid tumors are a well-known radiation-induced entity for both humans and mice; however, relatively little is known about genetic variants that increase susceptibility to this disease in mice. In HS/Npt mice, spontaneous thyroid adenomas occurred at relatively low frequencies and had a uniformly late onset, with tumors occurring between 700 and 800 days of age (Fig. 2A). In contrast, thyroid tumors arising in HZE ion– or γ-ray–exposed mice occur with significantly earlier onsets, with tumors arising as early as 250 days of age (Fig. 2A).

Association mapping reveals a significant 3.4-Mb interval on chromosome 2 for HZE ion–exposed animals (Fig. 2, B and C). The same locus is identified in the γ-ray–irradiated population if the significance threshold is decreased to a level at which 30% of identified QTL will be false positives. Combining both irradiated populations markedly increases the significance of the QTL identified on

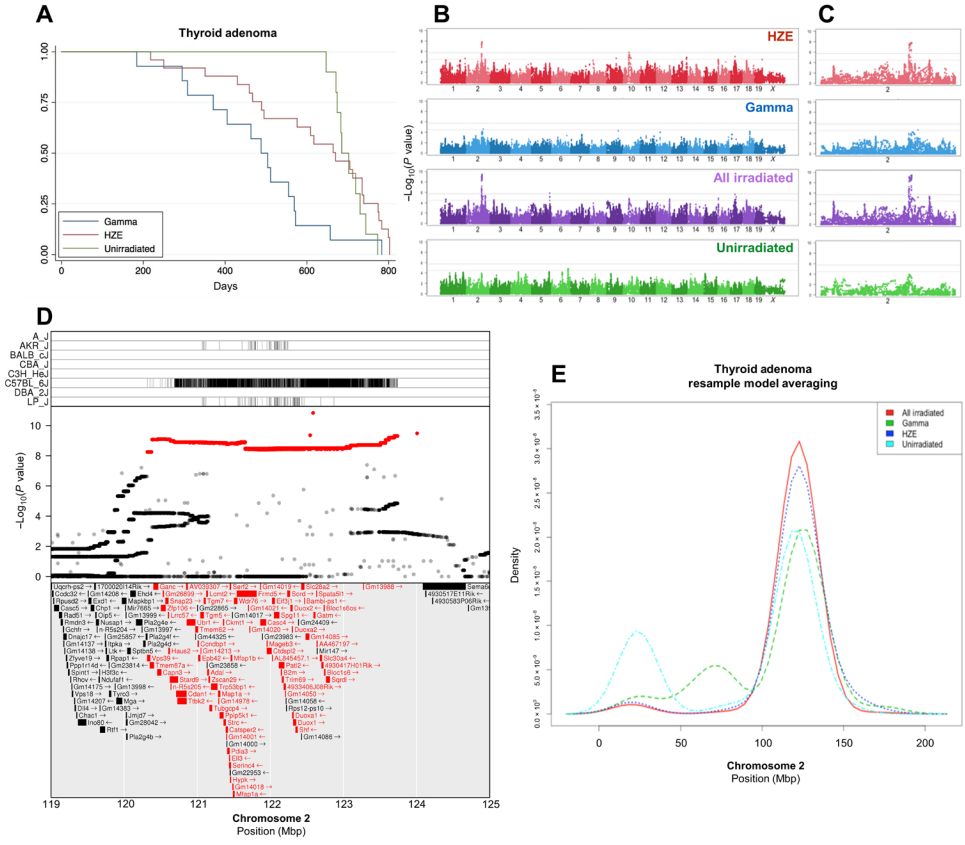

Fig. 2. Genome-wide association mapping identifies a susceptibility locus for thyroid adenoma shared by exposure groups. Thyroid follicular adenoma Kaplan-Meier survival estimate (**A**) along with genome-wide association plots for thyroid adenoma in HZE ion–irradiated, γ-ray–irradiated, HZE ion– and γ-ray–irradiated, and unirradiated mice (**B**) and an expanded plot for chromosome 2 (**C**), which contains the most significant association locus; gray lines indicate 95% (upper line) and 90% confidence (lower line) for $-\log_{10}(P$ values). Genome-wide association results reveal significant results in HZE ion– and γ-ray–irradiated mice that are further bolstered by combining the groups. The top panel of (**D**) shows strains that contribute the reference allele for the SNPs highlighted in red in the middle panel, indicated by vertical lines (D); the C57BL/6J strain contributes an allele that differs significantly from the other seven strains. The middle panel shows the $-\log_{10}(P$ value) of each SNP in the interval (D); the most significant SNPs are highlighted in red, and the bottom panel lists genes within the QTL interval. Genes that contain splice site, missense, or stop-related SNPs are colored red (D). Resample model averaging was performed within chromosome 2 to compare the distribution of peak $-\log_{10}(P$ values) for each exposure group (**E**); there is broad overlap for HZE- and γ-ray–irradiated mice, and grouping all irradiated mice together further narrows the distribution of peak $-\log_{10}(P$ values). Mbp, megabase pair.

chromosome 2. The QTL interval (119 to 125 Mb) contains 39,179 SNPs (Sanger Mouse Genomes, REL-1505) and 142 genes (Ensembl version 85) (Fig. 2D). Within the QTL region, the C57BL/6J parental strain contains an introgression from the *Mus musculus musculus* genome (*31*); we found that HS/Npt mice carrying the C57BL/6J haplotype at the QTL have increased thyroid tumor incidence regardless of whether they are exposed to HZE ions or γ-rays.

To further explore the possibility that the QTL identified on chromosome 2 controls susceptibility following γ-ray and HZE ion exposures, we used a nonparametric resample model averaging procedure (*32*) across the entire chromosome to identify genomic loci that consistently reappear in resampled populations. Briefly, genome scans are repeated for each new dataset created, in which some individuals may be sampled more than once and some not at all (*32*). Resample model averaging consistently identifies the same locus for all groups of mice, regardless of radiation exposure (Fig. 2E). Furthermore, the resample model averaging procedure identifies the same locus for tumors arising spontaneously (Fig. 2E). Data from this tumor phenotype indicate that the same inheritable genetic variants contribute to an individual's risk of developing thyroid cancer, regardless of radiation exposure.

Chromosomal leukemogenic events are similar following HZE ion or γ-ray exposure

Acute myeloid leukemia (AML) is another common radiation-induced tumor in both mice and humans (*33*, *34*). In concordance with previous studies conducted with inbred mice (*26*), γ-ray exposures in HS/Npt mice are more efficient at inducing AML than HZE ion exposures. In our γ-irradiated mice, 15.6% (96 of 615) developed AML compared to 2.9% (18 of 622) of those exposed to HZE ions and 1.6% (10 of 613) of unirradiated mice. AML median survival times were similar for all groups (Fig. 3A). Association mapping revealed a significant QTL for the γ-irradiated population on chromosome 2 that reached the 95% confidence threshold (Fig. 3, B and C), but no QTL was observed for the HZE ion–exposed population, in which the incidence of AML was much lower. However, when grouping HZE ion– and γ-ray–irradiated mice together, the same QTL was significantly bolstered (Fig. 3B). If the susceptibility alleles

identified at this locus were only contributing to disease following γ-ray irradiation and were, therefore, randomly distributed among the affected mice in the HZE ion–exposed group, then we would expect the $-\log_{10}(P$ values) to decrease when combining γ-irradiated mice; however, the $-\log_{10}(P$ value) for this locus significantly increases when repeating the mapping procedure included all irradiated mice.

Radiation-induced AML is a well-characterized disease in mice (*10*, *35*, *36*) and is most commonly the result of a radiation-induced minimally deleted region on chromosome 2 containing the *PU.1* gene (current murine nomenclature, *Spi1*) and a recurrent point mutation that inactivates the remaining *Spi1* allele (*37*). Figure 3C depicts mouse chromosome 2 with the positions of the QTL identified in our irradiated mice and the *Spi1* gene. To test the hypothesis that AMLs occurring in HZE ion–exposed animals will contain the same molecular aberrations know to occur in AML arising in γ-ray–exposed mice, the copy number for *Spi1* was investigated in leukemia samples to assess for deletions. As expected, most of the leukemias occurring in γ-ray–exposed mice had a deletion in one copy of *Spi1*. In contrast, *Spi1* deletions in spontaneously occurring AML were less common (Fig. 3D). Similar to γ-ray–irradiated mice, leukemias that developed in mice exposed to HZE ions, although fewer in number, also have an increased incidence of *Spi1* deletion. This finding indicates that AML arises by similar molecular mechanisms following exposures to HZE ions or γ-rays.

Because the QTL identified on chromosome 2 is approximately 60 Mb from the commonly deleted region containing *Spi1* and because radiation-induced deletions can be notoriously large, we considered the possibility that the identified QTL was also deleted in these leukemias, resulting in loss of one copy of the QTL region. To test this hypothesis, we determined the copy number for a gene located at distal to the QTL support interval, *Asxl1*. As expected, we found that *Asxl1* was not deleted in any sample in which *Spi1* was not deleted; however, in 69% of cases with a *Spi1* deletion, *Asxl1*—and presumably the entire QTL region—was also deleted (Fig. 3D). This demonstrates that most of the radiation-induced AML cases arose from progenitor cells haploinsufficient for the entire QTL region.

Harderian gland adenocarcinoma mapping reveals a QTL specific to HZE ion exposures

HZE ion and, to a lesser extent, γ-ray irradiation were particularly effective in inducing Harderian gland tumors at the doses used in this study, which was expected on the basis of extensive published

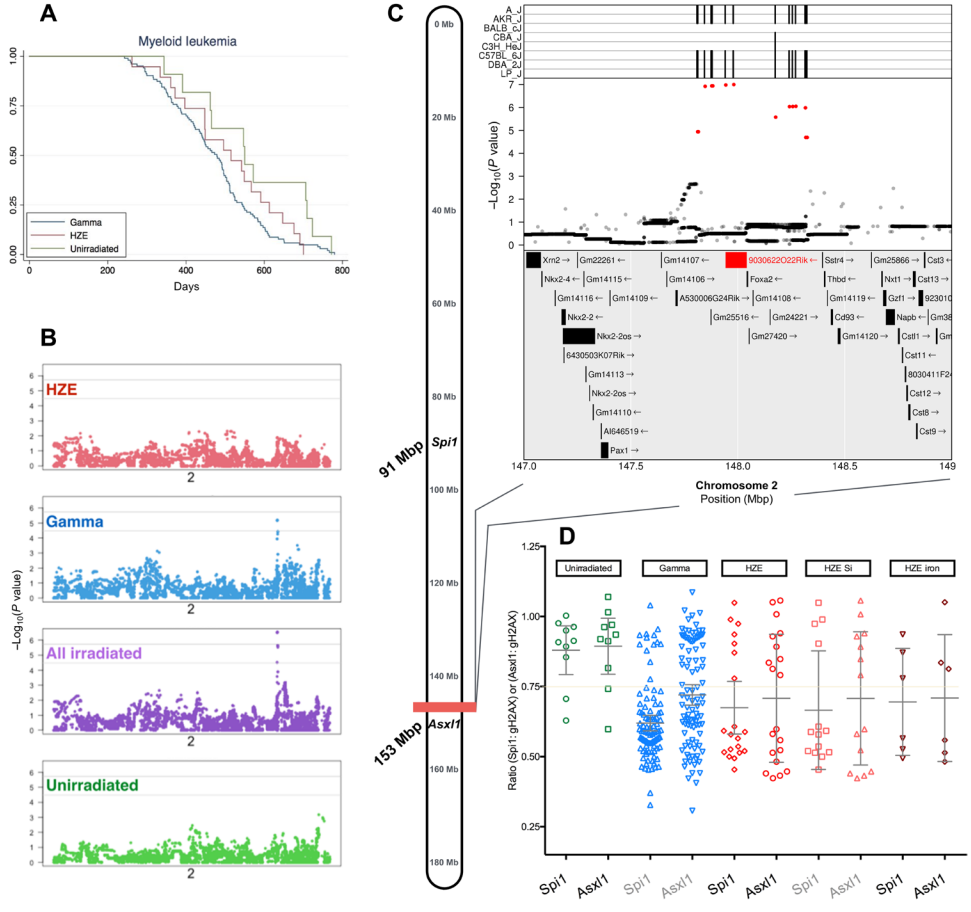

Fig. 3. A radiation-associated chromosomal deletion contains a susceptibility locus for myeloid leukemia. (**A**) Kaplan-Meier plots for myeloid leukemia demonstrate similar median survival estimates for myeloid leukemia between groups. (**B**) Genome-wide association procedures identify a narrow QTL on chromosome 2; two gray lines indicate 95% (upper line) and 90% confidence (lower line) for $-\log_{10}(P$ values). Expanded mapping results are depicted in (**C**) along with contributing strains for the reference allele. The A/J, AKR/J, C57BL/6J, DBA/2J, and LP/J strains contribute alleles that differ from the other strains, indicated by vertical lines in the top panel (C). The middle panel shows the $-\log_{10}(P$ value) of each SNP in the interval. The most significant SNPs are highlighted in red. The bottom panel shows the genes in the QTL interval. Genes that contain splice site, missense, or stop-related SNPs are indicated in red. Copy number results for *Spi1* and *Asxl1* in splenic samples from mice diagnosed with myeloid leukemia are plotted by exposure group (**D**).

radiation quality data on these tumors (*8*, *38*). In the HZE ion–irradiated group, Harderian gland tumors were observed in 22.7% (221 of 622) of mice and 3.2% (20 of 622) were malignant. In the γ-irradiated group, 15.3% (94 of 615) of mice developed Harderian gland tumors and 2.7% (17 of 615) were malignant. In contrast, spontaneous Harderian gland tumors occurred in only 4.1% (25 of 613) of unirradiated mice and 0.7% (4 of 613) were malignant. Despite the differences in tumor incidences following irradiation, median survival times for Harderian gland adenocarcinoma were similar for all groups (HZE ion, 582 days; γ-ray, 571 days; and unirradiated mice, 571 days).

Two QTL were observed for Harderian gland adenocarcinomas in HZE ion–irradiated mice, one on chromosome 4 and another on chromosome 9 (Fig. 4A). The 1.7-Mb interval identified on chromosome 4 (Fig. 4B) is similar to previously discussed QTL regions in that combining both irradiated populations markedly increases the significance of this locus, which suggests that this QTL is associated with Harderian gland adenocarcinoma susceptibility in both HZE ion– and γ-ray–irradiated mice. In contrast, a 2.3-Mb QTL interval on chromosome 9 is observed only in HZE ion–irradiated mice, and the locus is absent when combining all irradiated mice and repeating the mapping procedure (Fig. 4C). To further evaluate these QTL, resample model averaging was performed within chromosomes 4 and 9 to determine the distribution of peak $-\log_{10}(P$ values) along each chromosome. For chromosome 4, there is substantial spatial overlap identified in peak $-\log_{10}(P$ value) associations in the HZE ion–exposed population and the γ-ray–irradiated population, and the HZE ion– and γ-ray–irradiated population yields the most consistent identification of the QTL region (Fig. 4D). In contrast, although nearly all identified peak $-\log_{10}(P$ values) were identified in the 2.3-Mb QTL interval on chromosome 9 for HZE ion–irradiated mice, the distributions of peak $-\log_{10}(P$ values) for other exposure groups do not substantially overlap and are widely distributed along the chromosome (Fig. 4E). The resample model averaging results indicate that while the chromosome 4 QTL contributes to susceptibility to Harderian gland adenocarcinomas in both HZE ion– and γ-ray–irradiated populations, the QTL identified on chromosome 9 appears to only be involved in Harderian adenocarcinoma susceptibility following HZE ion exposures.

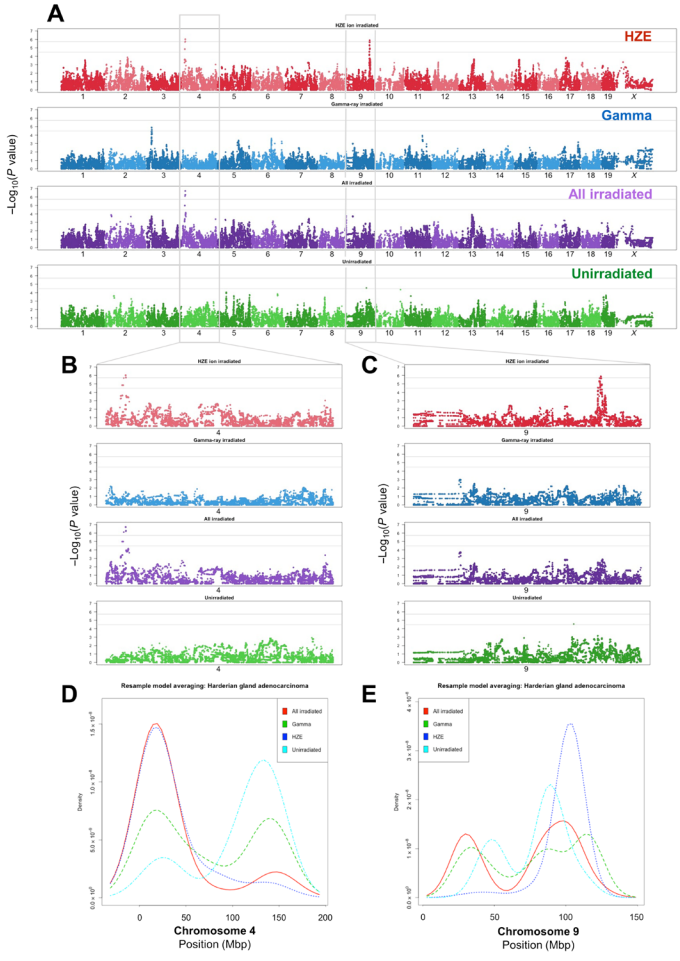

Fig. 4. Genome-wide associations for Harderian gland adenocarcinomas identify QTL common to both irradiation groups and specific to HZE exposures. Genome-wide association plots for Harderian gland adenocarcinoma (**A**) for HZE ion–irradiated, γ-ray–irradiated, HZE ion– and γ-ray–irradiated, and unirradiated mice; two gray lines indicate 95% (upper line) and 90% confidence (lower line) for $-\log_{10}$ (*P* values). Chromosome 4, which is expanded in (**B**), reveals a significant QTL associated with HZE ion irradiation, which is further increased significantly when grouping all irradiated mice (HZE ion and γ-ray irradiated) together, which indicated that the genetic variants in this location are important for Harderian gland adenocarcinoma following exposures to either HZE ion or γ-ray irradiation. In contrast, chromosome 9, which is expanded in (**C**), reveals a significant QTL associated only with HZE ion irradiation; this locus is absent when grouping all irradiated mice (HZE ion and γ-ray irradiated) together, which suggests that the allele(s) present in this region may only play a role for HZE ion–induced tumors. Resample model averaging was performed within chromosomes containing significant QTL. There is significant spatial overlap identified on chromosome 4 for peak $-\log_{10}(P$ value) associations in the HZE ion–exposed population, the γ-ray–irradiated population, and the HZE ion– and γ-ray–irradiated population that demonstrates the most consistent identification of the QTL region (**D**). In contrast, although nearly all identified peak $-\log_{10}(P$ values) were identified in the chromosome 9 QTL interval for HZE ion irradiated mice, the peak $-\log_{10}(P$ values) for other exposure groups are widely distributed along the chromosome (**E**).

Hierarchical clustering of genome-wide association scans indicates QTL similarity between histotypes regardless of radiation exposure

In addition to looking for similarities between individual, selected QTL for HZE ion– and γ-ray–exposed populations, we also sought a more holistic method in which entire genome-wide association results could be compared between groups in an unsupervised process. We used hierarchical clustering to create cluster dendrograms using entire genome-wide scans for a given phenotype. By considering results from genome-wide associations, rather than individualized peaks observed within genome-wide associations, we submit for comparison not only highly significant QTL regions but also the numerous loci detected with lower confidence.

Unsupervised hierarchical clustering of genome scans creates significant clustering events that often occur for the same histotype regardless of radiation exposure (Fig. 5A). Multiple tumor histotypes—including mammary adenocarcinoma, thyroid adenoma, and hepatocellular carcinoma—cluster by histotype, regardless of radiation exposure. To demonstrate and validate the methodology of QTL clustering, genome-wide scans for coat colors in each treatment group are evaluated and coat color genome-wide scans cluster together, as expected (Fig. 5B). These results further support the hypothesis that host genetic factors are highly important in determining risk

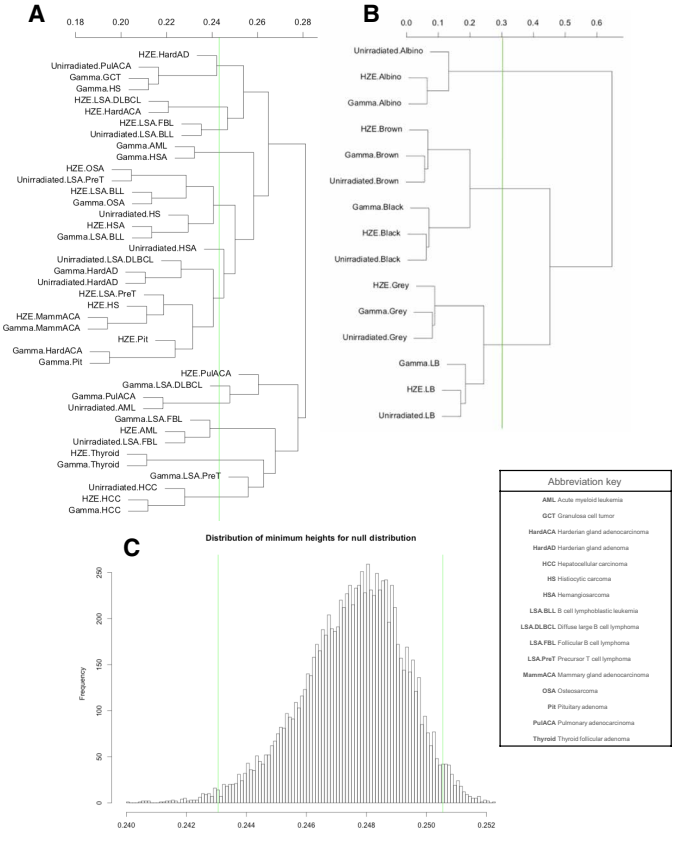

Fig. 5. Genome-wide association study data do not cluster by radiation exposure but by histotype for some tumors. (**A**) Unsupervised hierarchical clustering of genome-wide association scans for tumor phenotypes reveals that the most significant clustering events often occur for the same histotype regardless of radiation exposure; these include mammary adenocarcinoma, thyroid adenoma, and hepatocellular carcinoma. (**B**) As expected, clustering genome scans for coat color demonstrates the expected results: that genome scans cluster together despite exposure group. The green line represents the 99% confidence level of the most significant dendrogram heights by permutations ($-\log_{10}$ values permuted with genetic markers) to determine a distribution of dendrogram heights under the null hypothesis that no associations exist (**C**), demonstrating that the observed clusters are highly unlikely to occur randomly.

of radiation carcinogenesis, whether following HZE ion or γ-ray exposures.

Rate of metastasis is similar in HZE ion– or γ-ray–irradiated mice and unirradiated mice

Permissible exposure limits for astronauts are based on the risk of death from cancer rather than cancer development, and the incidence to mortality conversion used in the risk calculation uses spontaneously occurring cancers in the U.S. population. Thus, there is an assumption that radiogenic tumors are no more lethal than spontaneous tumors. To determine whether tumors that arise following HZE ion exposure are more malignant than their counterparts arising in unirradiated or γ-ray–irradiated mice, metastatic disease was characterized for each group. Pulmonary metastases were consistently observed in cases of hepatocellular carcinoma, Harderian gland adenocarcinoma, osteosarcoma, and ovarian granulosa cell tumor. Metastases were no more frequent in irradiated animals than in controls, and there was no significant difference in metastatic incidence between HZE ion–irradiated mice and γ-ray–irradiated mice (fig. S5A), and pulmonary metastatic density is similar between groups (fig. S5, B to D).

Tumor latency following irradiation was compared between exposure groups using survival statistics. Differences in tumor latency in this context indicate a decrease in time for tumor initiation or promotion. Since radiation is efficient at both initiation and promotion, decreased latencies are expected for irradiated population. Tumor progression is not evaluated, and our results therefore do not demonstrate whether tumors arising in irradiated individuals are more likely to progress rapidly than those arising spontaneously. As expected, tumors arising in both HZE ion– and γ-ray–irradiated mice show significantly decreased latencies in comparison to the unirradiated population (fig. S7 to S22). However, HZE ions did not further decrease latencies when compared to γ-ray–irradiated mice.

DISCUSSION

Carcinogenesis as a result of space radiation exposure is considered the primary impediment to human space exploration (*2*). Compared to forms of radiation found naturally on Earth, including x-rays, γ-rays, and β particles, HZE ions in space are much more difficult to shield (*2*) and have a distinct ionization pattern that aligns along dense track structures, resulting in clustered damage to chromatin (*6*). Because HZE ions, a highly penetrating component of GCRs, are not amenable to shielding (*28*, *29*), exposure risks are inherent to manned missions in interplanetary space, but estimating the risk associated with this unique form of particle radiation is complicated by the essential lack of data for human exposures (*28*). As a substitute, human exposure data from other forms of ionizing radiation, primarily γ-ray (*3*–*5*) photon radiation, are used in cancer risk models with the assumption that photon and particle radiation have qualitatively comparable biological effects.

Animal models are a vital component in determining the validity of the extrapolation of human terrestrial radiation exposure data to exposures that will occur in astronauts in the space radiation environment. To date, carcinogenesis studies designed to evaluate the effects of HZE ions have used rodents with limited genetic heterogeneity (*9*–*16*). The advantage of removing genetic variability in animal models is the consequent decrease in phenotypic variability, which allows for fewer individuals to detect potential environmental effects on phenotype; the disadvantage is that strain-specific responses in genetically identical populations are significant and can obscure the variability that one might expect in a diverse population, such as humans. By using a genetically diverse population with a wide range of tumor susceptibilities, the spectra of tumors that occur following exposures to particle and photon radiation can be compared. The results of this study indicate that the spectrum of tumor histotypes observed in a genetically diverse population exposed to particle radiation is not unique to that observed in a population exposed to photon radiation or to the tumor spectrum observed in an unirradiated population. Despite the similarities observed in tumor spectra following radiation exposures, the radiation qualities and doses used for this study have unique efficiencies at producing specific tumor types, and while this work demonstrates that the underlying genetics of susceptibility can be similar for tumorigenesis following both high- and low-LET radiation, further work is necessary to define risks for specific tumor histotypes based on exposures.

This study uses a highly recombinant mouse population (HS/Npt stock) that is genetically diverse and designed for genome mapping (*19*–*21*, *23*), a forward-genetics approach that allows for an unbiased search of the entire genome for genetic associations. In contrast, genetically engineered mouse models rely on a reverse-genetics approach in which a given gene is first altered and the resulting phenotypes are then characterized. Studies using forward-genetics are most informative in populations that contain abundant genetic and phenotypic diversity. HS/Npt mice are a multiparent cross derived from eight inbred strains (A/J, AKR/J, BALBc/J, CBA/J, C3H/HeJ, C57BL/6J, DBA/2J, and LP/J); each individual contains a unique mosaic of founder haplotypes and a high degree of heterozygosity, and recombination events become increasingly dense with each generation. Our population of HS/Npt mice was obtained from generation 71 of circular outbreeding. Creating these populations is not trivial and has been a central goal of communities involved in genetics research over the past few decades, resulting in the creation of rodent populations ideal for genome mapping (*18*–*20*, *39*–*42*).

Genome mapping allows the discovery of QTL associated with susceptibility to complex traits, such as radiogenic cancers; this approach is uniquely suited to comparing inheritable risk factors for cancers following exposures to unique carcinogens, such as particle and photon radiation. In broader terms, this work demonstrates the utility of highly recombinant mouse models created for genetic mapping in carcinogenesis studies, an application that has not been previously attempted. Mapping QTL in carcinogenesis studies provides inherent challenges due to the structure of binomial data, potential confounding causes of death following irradiation and aging, the fundamental stochastic nature of radiation tumorigenesis, and incomplete penetrance of potential allelic variants. Despite these challenges, we were able to map QTL for 13 neoplastic subtypes and many of these identified loci are previously unidentified.

At the doses used in this study, HZE ions appear to be less effective than γ-rays in inducing precursor T cell lymphoblastic lymphoma (pre-T LL) and ovarian tubulostromal adenomas and granulosa cell tumors. This may be due to a combination of dose inhomogeneity in HZE ion–irradiated tissues and the major role cell killing plays in the etiology of these specific tumors. pre-T LL can be prevented by transplanting irradiated mice with unirradiated syngeneic bone marrow cells or by shielding some of their bone marrow during irradiation (*43*, *44*). The underlying mechanism by which unirradiated bone marrow cells suppress lymphomagenesis may involve a cell competition process by which older T cell progenitors resident in the thymus are normally replaced by fresh progenitors that immigrate from the bone marrow. Radiation kills these fresh bone marrow cells or reduces their fitness, which, in turn, prolongs the time that older T cell progenitors already in the thymus survive and self-renew. This, along with the increased proliferative cycles of the older T cell progenitors needed to maintain production of mature T cells, results in a corresponding increase in the oncogenic mutations that they accumulate and a concomitant increase in lymphomagenesis (*45*). Replenishing dead or damaged bone marrow cells by transplantation or preventing their damage through shielding suppresses lymphomagenesis.

At the 3-Gy dose of γ-rays used in this study, all of the bone marrow cells are uniformly irradiated. This is not the case for HZE particle radiation. The average diameter of a murine bone marrow cell nucleus is around 6 μm (*46*). At the fluence of HZE ions used in this study, the probability that a 6-μm-diameter nucleus will be traversed by a ^{28}Si ion and a ^{56}Fe particle is 0.88 and 0.40, respectively. On the basis of a Poisson distribution, the probabilities of a nucleus not being traversed at all are 0.41 and 0.67 for ^{28}Si and ^{56}Fe irradiation, respectively. Thus, many of the T cell progenitors in the bone marrow are not irradiated (although they receive a small dose from γ-rays). These cells should exert a protective effect similar to transplanting unirradiated bone marrow cells or shielding some of the bone marrow during irradiation, rendering HZE ions less efficient for lymphomagenesis. Given that most of the pre-T LL in the HZE ion–irradiated group are likely spontaneous, it is expected that they cluster more closely to spontaneous pre-T LL than to γ-ray–induced pre-T LL.

The mechanism leading to murine tumors of ovarian surface epithelium origin is well understood. Loss of primordial follicle oocytes by radiation-induced apoptosis results in a decrease in estrogen production, which, in turn, leads to elevated levels of follicle-stimulating hormone (FSH) and luteinizing hormone (LH) in the circulation. FSH and LH drive proliferation of ovarian surface epithelium cells (*47*). Ovarian tumors can be induced in some animal models by artificially manipulating levels of these hormones (*47*–*49*). Irradiated mice can be protected from tubulostromal adenomas and granulosa cell tumors by shielding one ovary during irradiation or by transplanting the mice with an unirradiated ovary (*50*, *51*); these interventions protect some oocytes and thereby maintain proper regulation of FSH and LH levels.

Assuming that the target cells are primordial follicle oocytes with a diameter of 12 μm, the probabilities of no traversals are 0.2 for ^{56}Fe and 0.03 for ^{28}Si at the 0.4-Gy dose used here. The probabilities for one or fewer traversals are 0.52 for ^{56}Fe and 0.14 for ^{28}Si. Whether a sufficient number of follicles survive at 0.4 Gy to account for the observed ovarian tumor sparing is unknown. Mishra and colleagues (*52*) observed a dose-dependent decrease in primordial stage follicles in C57BL/6 mice 8 weeks after irradiation with ^{56}Fe ions (600 MeV/n). Sixteen percent of the follicles survived at the 0.3-Gy dose, and normal levels of serum FSH and LH were present; at 0.5 Gy, only 1% of the follicles survived and an increase in serum FSH was observed. Caution is needed in using Mishra's results in interpreting our own since we used mice with different genetic backgrounds and the FSH and LH levels in the 0.3 Gy–irradiated mice may increase relative to unirradiated controls if time points beyond 8 weeks are assayed. In any event, microdosimetric effects should be incorporated into any risk model for tumors in which cell killing plays a prominent role.

The location of the chromosome 2 QTL in a region frequently deleted in radiogenic AMLs may be happenstance, but there are scenarios in which its chromosomal location would be crucial to its function. One possibility is that the polymorphism increases the frequency of AML-associated chromosome 2 deletions in irradiated hematopoietic cells by controlling the spatial confirmation of the chromosome such that the proximal and distal deletion breakpoints are in close proximity to one another (*46*). This type of proximity mechanism has been evoked to explain recurrent chromosomal rearrangements seen in radiation-induced papillary thyroid carcinoma and some spontaneous cancers (*53*, *54*). In this scenario, the QTL could be a structural polymorphism (e.g., segmental duplication or interstitial telomeric sequence), which would affect chromosomal conformation, yielding a different conformation in susceptible mouse strains than resistant strains. Structural polymorphisms are easily missed in the assembly of the strain-specific genomic sequences

used for mapping studies, so we would be unaware of its existence. A second possibility is that the polymorphism is in a gene needed for myeloid progenitor cell survival. Mouse strains resistant to myeloid leukemia would have a hypomorphic allele of this gene. If one copy is lost (i.e., through radiation-induced deletion), then the remaining copy would be insufficient for cell survival. Thus, in mouse strains resistant to radiogenic AML, a chromosome 2 deletion, which is the first step in radiation leukemogenesis, is a lethal event and leukemogenesis is thereby halted. Susceptible strains would have a fully functional allele of the gene, so that if one copy is deleted, the remaining copy maintains cell viability, allowing further leukemogenic events to occur (*46*). A caveat to both the chromosome conformation and haploinsufficiency scenarios is that the chromosome 2 deletions mapped in radiogenic AMLs from the F1 progeny of AML-susceptible CBA/H mice and AML-resistant C57BL/6 mice do not occur preferentially in the CBA/H origin chromosome (*55*). However, in that study, only 10 tumors were informative. In addition, susceptibility to radiogenic AML is multigenic, so it is possible that the difference in susceptibility between the CBA/H and C57BL/6 strains is not due to the chromosome 2 QTL.

HZE ions seem particularly effective in inducing Harderian gland tumors at the doses used in this study. This result was expected on the basis of extensive published radiation quality data on these tumors (*8*, *38*). The mechanism responsible for higher tumorigenic efficacy of HZE ions relative to γ-rays is unknown; however, we have identified a QTL associated with Harderian gland adenocarcinoma following HZE ion exposures that does not appear to lend susceptibility to the same tumor following γ-ray exposures (Fig. 4C). Furthermore, HZE ion–induced Harderian gland adenomas and adenocarcinomas cluster away from spontaneous and γ-ray–induced Harderian gland tumors (Fig. 5), indicating non-overlap of some of the susceptibility loci. There are data that suggest that HZE ion irradiation has an effect on tumor promotion that γ-ray irradiation lacks. The observation is that pituitary isografts, which result in elevated levels of pituitary hormones, enhance the induction of Harderian gland tumors and decrease their latency in mice irradiated with γ-rays or fission neutrons but do not increase tumor prevalence in mice irradiated with ^{56}Fe ions (600 MeV/n) (*12*). This would explain the high relative biological effectiveness (RBE) for ^{56}Fe ions. It would also render QTLs that act in the promotion of γ-ray and spontaneous tumors irrelevant to HZE ion–induced tumors.

The use of unsupervised clustering on genome-wide association results is a novel approach to search for shared tumorigenic mechanisms between radiogenic and spontaneous tumors or between tumors induced by different radiation qualities. Potentially, the results could be used to inform risk modeling. For example, using the 99% confidence interval as a cutoff, thyroid adenomas, pituitary tumors, osteosarcomas, B cell lymphoblastic leukemia, mammary tumors, and hepatocellular carcinomas cluster by histotypes regardless of whether they arose in HZE ion–irradiated or γ-ray–irradiated mice. Of these, the incidences of thyroid tumors, pituitary tumors, and osteosarcomas are significantly increased following exposures to either HZE ions or γ-rays. Taking pituitary adenoma as an example, these findings suggest that it would be reasonable to extrapolate the risk of HZE ion–induced pituitary adenoma as a multiple of γ-ray–induced pituitary adenoma risk (i.e., using a relative risk model). Because there were too few spontaneous pituitary adenomas to position them on the dendrogram, we cannot determine whether the risk of HZE ion–induced pituitary adenoma could reasonably be modeled on the basis of the incidence of the spontaneous tumor. Another pattern of association is observed for Harderian gland adenoma and follicular B cell lymphoma in which, at the 99% confidence interval, spontaneous tumors cluster with γ-ray–induced tumors but not with HZE ion–induced tumors. There are a number of ways that this could occur. Three possibilities are as follows: (i) HZE ions act through a tumorigenic mechanism different from that of spontaneous and γ-ray–induced tumors. (2) HZE ions bypass the need for one or more of the genetically controlled steps required for spontaneous and γ-ray–induced tumors, and (iii) there are multiple pathways to tumor formation, and HZE ion irradiation forces tumorigenesis through only one (or a subset) of them. Harderian gland tumors may fall into the second possibility. As described earlier, observations on mice receiving pituitary isografts before irradiation suggest that HZE ions may have Harderian gland tumor promotion effects that γ-rays lack. If so, the QTL controlling those effects would be inconsequential in the tumorigenesis of HZE ion–induced Harderian gland tumors, and those tumors would cluster away from their spontaneous and γ-ray–induced counterparts. Whether a relative risk model, an absolute risk model, or a combination of the two would be most appropriate in Harderian gland tumor risk calculations would depend on which of the above possibilities is most accurate.

NASA seeks to limit the risk of exposure-induced death (REID) from radiogenic cancer to below 3% (*56*). For multiple missions aboard the International Space Station (flown in solar minimum conditions), the model projects that males will exceed permissible exposure limits at 24 months and females, at 18 months; women are considered at greater risk for radiogenic cancers than men because of longer life spans and increased susceptibility to specific cancer types, including lung, ovarian, and breast carcinomas. Because the 3% REID is derived from the upper 95% confidence interval for the risk estimate (*57*), decreasing the uncertainty for space radiation–induced cancers can significantly increase the flight time allowed for astronauts. The 95% confidence interval surrounding the risk estimates not only primarily reflects uncertainties in our understanding of HZE ions but also includes uncertainties surrounding dose-rate effects, transfer of risk between human populations, space dosimetry, and errors in the existing human epidemiology data. Concerning sex predilections, our results also demonstrate a sex difference in carcinogenesis risk, where female mice are at greater risk for radiogenic cancers than males, following either HZE ion or γ-ray exposures. These results are consistent with the current NASA model to calculate cancer risk from space radiation exposures (*5*).

Whether genotypic assays of radiosensitivity can improve the precision of risk assessment in humans will depend on a number of factors. One is the extent to which heritable sequence variants determine cancer risk from HZE ion exposures. HZE ion radiation exposures result in more complex molecular lesions that are less amenable to repair (*58*). Thus, it could be argued that sequence variants that result in subtle differences in DNA repair and damage response pathways would have a lesser impact on HZE ion radiation carcinogenesis. However, this work demonstrates that genetic susceptibility does indeed have a significant role in tumorigenesis following HZE ion exposures. Personalized approaches to cancer risk assessments may eventually allow for greater reductions in uncertainties when generating space radiation cancer risk estimates (*28*).

There are limitations to a mouse carcinogenesis study comparing acute γ-ray and HZE ion exposures. First, for cost efficiency and

logistics reasons, a single dose was used for each radiation quality: 3.0 Gy for γ-ray exposures and 0.4 Gy for HZE ion exposures. Preliminary studies have demonstrated that these doses produce the maximum tumor incidence in inbred strains (*24*). Because tumor susceptibility and association mapping were the primary goals of this study, doses were chosen with the goal of generating the greatest tumor incidences and, therefore, the greatest power to detect significant QTL. However, caution must be taken when comparing the two single-dose groups, as it is impossible to untangle dose responses in such a study. An additional benefit of the selected doses is that 0.4 Gy of HZE ions represents a realistic dose, received over 20 to 30 months, for a flight crew traveling to Mars. Second, the applicability of these findings to human populations is limited, as rodents serve only as models of carcinogenesis.

The results presented here indicate that host genetic factors dictate risk for tumor development following radiation exposures, regardless of radiation quality. Therefore, at a population level, risks can be extrapolated from terrestrial exposures to the space radiation environment and at an individual level, and humans harboring susceptibility alleles for radiation-induced tumors developed on Earth are also likely at increased risk in space.

MATERIALS AND METHODS

Animals and radiation exposures

Male and female HS/Npt mice (n = 1850) were generated from breeding pairs obtained from Oregon Health and Sciences University (Portland, OR). The mice were group-housed (five mice of the same sex per cage) in a climate-controlled facility at 70°F (21.1°C) with free access to food (Teklad global rodent diet 2918) and sterile water and a 12-hour light cycle. Mice were shipped to Brookhaven National Laboratories (Upton, NY) where they were exposed to accelerator-produced HZE ions at the NASA Space Radiation Laboratory at 7 to 12 weeks of age. HS/Npt stock mice of both sexes were exposed to 0.4 Gy of ^{28}Si ions (240 MeV/n) (n = 308) or ^{56}Fe ions (600 MeV/n) (n = 314), 3 Gy of ^{137}Cs γ-rays (n = 615), or sham irradiated (n = 622). Following irradiation exposure or sham irradiations, mice were returned to Colorado State University (Fort Collins, CO) and monitored twice daily for the duration of the study. The mice were evaluated for cancer development until they reached 800 days of age or became moribund. All animal procedures were approved by the Colorado State University Institutional Animal Use and Care Committee.

HS/Npt mice

This study uses a highly recombinant mouse population (HS/Npt stock) that is genetically diverse and designed for genome mapping (*19*–*21*, *23*). HS/Npt mice are a multiparent cross derived from eight inbred strains (A/J, AKR/J, BALBc/J, CBA/J, C3H/HeJ, C57BL/6J, DBA/2J, and LP/J); each individual contains a unique mosaic of founder haplotypes and a high degree of heterozygosity, and recombination events become increasingly dense with each generation. Our population of HS/Npt mice was obtained from generation 71 of circular outbreeding.

Genotyping

DNA was isolated from tail biopsies taken from each mouse at 9 to 10 weeks of age. DNA was extracted and purified (QIAGEN, catalog no. 69506) according to the manufacturer's instructions. GeneSeek (Lincoln, NE) performed genotyping assays using the Mega Mouse Universal Genotyping Array (MegaMUGA) (*59*) for a total of 1878 mice (including 28 inbred mice representing the founder strains). The MegaMUGA is built on the Illumina Infinium platform and consists of 77,808 single-nucleotide polymorphic markers that are distributed throughout the genome with an average spacing of 33 kb.

Genome reconstruction as mosaics of founder haplotypes

The heterogeneous stock mice are descendants of eight inbred founder strains. For each mouse, allele calls from the MegaMUGA array were used to calculate descent probabilities using a hidden Markov model (HMM), in which the hidden states were the founder strains and the observed data were the genotypes. The HMM generates probabilistic estimates of the diplotype state(s) for each marker locus and produces a unique founder haplotype mosaic for each mouse (*18*).

Pathology

For this lifetime carcinogenesis study, all disease states were interpreted within the context of a systematic pathologic evaluation directed by board-certified veterinary pathologists (E.F.E. and D.A.K.). Structured necropsy and tissue collection protocols were followed for each mouse and involved photodocumentation of all gross lesions, collection of frozen tumor material, and preservation of tumor material in RNAlater. All tissues were grossly evaluated for all mice. To evaluate brain tissues and Harderian glands, craniums were decalcified for 48 hours in Formical-4 (StatLab, McKinney, TX 75069, product 1214) and five coronal sections of the skull were reviewed for each mouse. All gross lesions were evaluated microscopically and fixed in 10% neutral-buffered formalin and paraffin-embedded, and 5-μm sections were stained with hematoxylin and eosin (H&E) and evaluated by a veterinary pathologist. For mice with solid tumors, all lung fields were examined histologically to detect the presence or absence of micrometastases. Tumor nomenclature was based on consensus statements produced by the Society of Toxicologic Pathology for mouse tumors (www.toxpath.org/inhand.asp). Representative histologic images routinely stained with H&E are presented in figs. S2 (A to E) and S3 (A and B).

Immunophenotyping lymphoid neoplasms

Tissue microarrays were constructed to immunophenotype and subcategorize lymphoid neoplasms, which were the most commonly diagnosed tumors in irradiated and unirradiated HS/Npt mice. Identification of tissue sampling regions was performed by a veterinary pathologist. For each case, duplicate cores were taken from multiple anatomic locations (lymph nodes, spleen, thymus, etc.). Thirteen tissue microarrays were created, each of which contained six cores of control tissue at one corner of the array (haired skin, spleen, thymus, or liver); these control tissues were present in a unique combination and allowed for (i) orientation of the resulting sections, (ii) verification that the slide matched the block, and (iii) positive controls for immunohistochemistry. Figure S3D illustrates one tissue microarray as well as the resulting immunohistochemistry results for one thymic lymphoma (fig. S3E) and a core containing normal spleen (fig. S3F). Immunohistochemistry for T cell identification was performed using a rabbit monoclonal, anti-CD3 (SP7) antibody obtained from Abcam (ab16669; 1:300). Immunohistochemistry for B cell identification was performed using two rabbit monoclonal antibodies: an anti-CD45 antibody (ab10558;

1:1000) and an anti-PAX5 antibody (ab140341; 1:50). All immunohistochemistry was performed on a Leica BOND-MAX autostainer with the Leica BOND Polymer Refine Red Detection system (Leica DS9390, Newcastle Upon Tyne, UK). In addition to defining the immunophenotype, lymphomas were characterized according to the Mouse Model of Human Cancer Consortium's Bethesda protocols (*60*). For these protocols, anatomic location is important for the final diagnosis, and therefore, lymph node involvement was used from necropsy reports when necessary. Additional features included cell size, nuclear size, chromatic organization, and mitotic figure frequency, and the presence or absence of a leukemic phase was defined by bone marrow involvement within the sternum or femur. The most common lymphoma subtypes (fig. S4A) were evaluated for survival (fig. S4B), and pre-T LL typically presented with early-onset and large thymic masses.

Molecular characterization of AML

Droplet digital polymerase chain reaction (ddPCR) was performed on cases of AML to assess deletion status via copy number variation for two genes: *Spi1* and *Asxl1*. These genes are both located on chromosome 2 at base pair locations 91,082,390 to 91,115,756 for *Spi1* and 153,345,845 to 153,404,007 for *Asxl1*. To establish a reference for normal diploid copy number in each AML sample, the copy number of *H2afx* was also determined. *H2afx* is located on chromosome 9, and deletions in this region have not been reported in murine AML. Bio-Rad PrimePCR probes were used for all assays as follows: *Asxl1* ddPCR probe (dMmuCPE5100268), *Spi1* ddPCR probe (dMmuCPE5094900), and *H2afx* ddPCR probe (dMmuCPE5104287). Ratios were created between the test gene and the reference gene (*Spi1*:*H2afx* and *Asxl1*:*H2afx*) to determine copy number with the assumption that the reference gene would not be deleted or amplified. Ideally, ratios of 1:1 represent equal copy numbers for both the test gene and the reference gene, and ratios of 1:2 represent a deletion in one copy of the test gene. However, since the tumor samples contained neoplastic cells as well as stromal cells and other cells, the ideal 1:2 ratio was not commonly observed. This is because stromal cells, which occur at unknown proportions in each tumor and which should not have chromosomal deletions, artificially increase ratios for tumor samples in which a deletion is indeed present. To account for stromal cell contamination, a cutoff ratio of 3:4 was established. Tumor samples with ratios below 3:4 were considered to have a deletion in one copy of the test gene.

Metastatic disease quantification

For cases in which a solid tumor was identified, a standard section containing all lung lobes was processed and evaluated histologically. In cases where pulmonary metastases were observed, whole-slide scanning was performed at ×200 magnification using an Olympus VS120-S5 and the OlyVIA software suite (www.olympusamerica.com/) to generate images for quantification of metastatic density (fig. S5). An analysis software, ImageJ (https://imagej.nih.gov/ij/), was used to quantify the total area of normal lung and the total area of metastatic foci (fig. S5). Metastatic density is reported as a percentage of the total metastasis area divided by the total lung area.

Genome scans and QTL mapping

Association mapping was performed using a mixed-effects regression model with sex and cohort as fixed effects and a random-effects term to adjust for relatedness between mice by computing a matrix of expected allele sharing of founder haplotypes for each pair of mice (*22*). Three statistical models were fit to account for the wide range of trait distributions in this study. A generalized linear regression model was fit for binomial distributions, such as neoplasia. Cox regression analysis was incorporated to model time-to-event distributions to evaluate genetic contributions to tumor latency. Following genome-wide association analyses, resample model averaging methods were used to identify QTL that are consistently reproduced within subsamples of the mapping population.

Significance thresholds, confidence intervals, and effect sizes

Thresholds were determined using a permutation procedure in which the genotypes were fixed and the phenotype values were rearranged randomly within each sex. The distribution of the maximum negative log(P value) of association under the null hypothesis that no associations exist (null model) was determined for each genome scan with permuted data. One thousand permutations were performed for each phenotype in each radiation exposure group, simulating effects arising from covariates, the linkage disequilibrium structure of the genome, and effects due to phenotype distribution. A threshold was defined as an estimate of the genome-wide significance for which a type I statistical error will occur at a given frequency (*29*). Confidence intervals for each QTL were determined by nonparametric resample model averaging procedures using bootstrap aggregation with replacement. In this procedure, the mapping population is sampled to create a new dataset in which some individuals may be omitted and some may appear multiple times (*30*), and the locus with peak significance is recorded. Resampling is repeated 200 times for each phenotype to determine a 95% confidence interval for a given QTL. Effect sizes were calculated using the Tjur method for association mapping with logistic regression and pseudo-R^2 for mapping with Cox proportional hazard regression. Statistical significance for each model was assessed using a permutation strategy to randomize genotypes via resampling without replacement and maintaining covariates. Permutation analysis was performed (1000 tests) for each trait and exposure group to generate estimations of genome-wide significance thresholds. As genome scans with hundreds of thousands of imputed SNPs are computationally intensive, parallel computing was essential and accomplished using spot instances of resizable Elastic Compute Cloud hosting resources.

Using clustering procedures with whole-genome scans

Comparisons were made between whole-genome scans using Pearson correlations as a similarity measure with clustering based on average linkage. Significance of clustering results was estimated with 10,000 random permutations of the dataset (−log10 values permuted with genetic markers) to determine a distribution of dendrogram heights under the null hypothesis that no associations exist. Each permutated dataset simulates a null distribution of the maximally significant clustering based on a randomly assorted set of P values for each genomic locus.

Resample model averaging for comparative QTL analysis

Bootstrap aggregation is a resample model averaging procedure that has been demonstrated to produce highly accurate estimates of QTL in structured populations (*32*). The procedure is relatively simple: for a genome-wide association study (GWAS) of n individuals, a sampling of n draws is obtained, with replacement, from the observed

individuals to form a new dataset in which some individuals are omitted and some appear multiple times. For each new dataset created this way, an estimate of the QTL location is calculated. This process is repeated many times and is the basis for determining a confidence interval for a given result. The use of bootstrap procedures is commonly used this way to estimate QTL support intervals in experimental crosses; however, this statistical method can potentially be applied to other areas of QTL research, including comparative QTL mapping.

When an identical QTL is observed for two distinct traits, one explanation is that a single gene is involved for two distinct biologic processes, also known as pleiotropy. This was sometimes assumed in early mouse QTL studies that resulted in coincident loci for distinct traits. Another possibility, however, is that two distinct genetic variants are present in close proximity, each independently contributing to the two phenotypes. Because the two hypothetical genetic variants happen to be in close proximity, they are difficult to distinguish in low-resolution mapping studies. Using resample model averaging in highly recombinant mice is proposed to best differentiate precise locations of the QTL; if the same markers were repeatedly identified, then the case for pleiotropy was strengthened. For comparative QTL mapping in tumorigenesis studies, nonparametric resample model averaging could similarly be leveraged to identify whether the same QTL renders an individual susceptible to distinct environmental carcinogens. One significant advantage to using bootstrap procedures to detect potential coincident loci is that comparisons can be made between groups based on the identification of a highly significant QTL identified in only one exposure group (e.g., at a false-positive rate of 1 per 20 scans). This QTL may be present in the alternative exposure group, but at lower confidence (e.g., at a false-positive rate of 1 per 10 scans), and therefore discarded in a typical GWAS. A diagrammatic representation of the comparative QTL bootstrap procedure is presented in fig. S6. Because the resultant genetic positions derived from bootstrapping are composed of the most significant locus for each resampling regardless of the significance level for the mapping procedure, comparisons can be drawn between QTL that might have been discarded on the basis of the stringent statistical demands of an assay involving hundreds of thousands of independent tests. Using this procedure on thyroid tumors demonstrates that the same loci are consistently identified whether exposed to particle or photon irradiation (Fig. 2E). Using the comparative QTL procedure described, it can be determined whether an individual's cancer risk from one carcinogen will be predictive of that individual's cancer risk to another carcinogen. The application of this procedure is well illustrated by the space radiation problem, where much is known about γ-ray exposures and little is known about space radiation exposures.

Hierarchical clustering of genome scans

In addition to looking for similarities between individual selected QTL for HZE ion– and γ-ray–exposed populations, we also sought a more holistic method in which entire genome scans could be compared between groups in an unsupervised process. By using entire genome scans, we submit for comparison not only highly significant regions but also the numerous loci detected with lower confidence. To determine similarity of genetic association profiles for all phenotypes and to detect possible coincident QTL, clustering procedures were used to compare genome-wide association scans between different radiation exposure groups. To demonstrate and validate the methodology of QTL clustering, genome-wide scans for coat colors in each treatment group are evaluated (Fig. 5B). As expected, genome-wide scans for coat color are unaffected by radiation exposures, and therefore, clustering is based entirely on coat phenotype rather than radiation exposure group. Using the same procedure for neoplasia indicates that tumor types often clustered together as well, regardless of radiation exposure (Fig. 5A). Genome scans for thyroid tumors and mammary adenocarcinomas in radiation-exposed groups and all hepatocellular carcinoma genome scans cluster together. This finding supports the hypothesis that host genetic factors are more important in determining neoplasm incidence than radiation exposure type. Unlike other statistic procedures, such as regression models, clustering lacks a response variable and is not routinely performed as a formal hypothesis test. Therefore, determining the significance of a clustering result can be problematic, as no consensus method exists for cluster validation. Permutation analysis provides the distribution of clustering results that will randomly occur from a given dataset; this can then be used as a baseline from which to determine a significance level on a given dendrogram tree [green line in Fig. 5 (A to C)]. While the overall validity of a given cluster can be accomplished by cluster permutation analysis, no method is identified to estimate the number of clusters that should be present in a dataset. Furthermore, methods to determine the significance of specific subset of objects clustering together do not exist; in such cases, the permutation threshold is likely overly stringent.

SUPPLEMENTARY MATERIALS

Supplementary material for this article is available at http://advances.sciencemag.org/cgi/content/full/6/16/eaax5940/DC1

View/request a protocol for this paper from *Bio-protocol*.

REFERENCES AND NOTES

1. C. Zeitlin, D. M. Hassler, F. A. Cucinotta, B. Ehresmann, R. F. Wimmer-Schweingruber, D. E. Brinza, S. Kang, G. Weigle, S. Böttcher, E. Böhm, S. Burmeister, J. Guo, J. Köhler, C. Martin, A. Posner, S. Rafkin, G. Reitz, Measurements of energetic particle radiation in transit to Mars on the Mars Science Laboratory. *Science* **340**, 1080–1084 (2013).
2. M. Durante, F. A. Cucinotta, Heavy ion carcinogenesis and human space exploration. *Nat. Rev. Cancer* **8**, 465–472 (2008).
3. A. Berrington de Gonzalez, E. Gilbert, R. Curtis, P. Inskip, R. Kleinerman, L. Morton, P. Rajaraman, M. P. Little, Second solid cancers after radiation therapy: A systematic review of the epidemiologic studies of the radiation dose-response relationship. *Int. J. Radiat. Oncol. Biol. Phys.* **86**, 224–233 (2013).
4. UNSCEAR, *Sources and Effects of Ionizing Radiation Sources* (UNSCEAR, 2016), pp. 1–274.
5. F. A. Cucinotta, M. Alp, B. Rowedder, M. H. Kim, Safe days in space with acceptable uncertainty from space radiation exposure. *Life Sci. Space Res.* **5**, 31–38 (2015).
6. D. T. Goodhead, Spatial and temporal distribution of energy. *Health Phys.* **55**, 231–240 (1988).
7. S. Board, *Technical Evaluation of the NASA Model for Cancer Risk to Astronauts Due to Space Radiation* (National Research Council, 2012).
8. H. Bielefeldt-Ohmann, P. C. Genik, C. M. Fallgren, R. L. Ullrich, M. M. Weil, Animal studies of charged particle-induced carcinogenesis. *Health Phys.* **103**, 568–576 (2012).
9. K. Ando, S. Koike, C. Oohira, T. Ogiu, F. Yatagai, Tumor induction in mice locally irradiated with carbon ions: A retrospective analysis. *J. Radiat. Res.* **46**, 185–190 (2005).
10. M. M. Weil, J. S. Bedford, H. Bielefeldt-Ohmann, F. A. Ray, P. C. Genik, E. J. Ehrhart, C. M. Fallgren, F. Hailu, C. L. Battaglia, B. Charles, M. A. Callan, R. L. Ullrich, Incidence of acute myeloid leukemia and hepatocellular carcinoma in mice irradiated with 1 GeV/nucleon ^{56}Fe ions. *Radiat. Res.* **172**, 213–219 (2009).
11. T. Imaoka, M. Nishimura, S. Kakinuma, Y. Hatano, Y. Ohmachi, S. Yoshinaga, A. Kawano, A. Maekawa, Y. Shimada, High relative biologic effectiveness of carbon ion radiation on induction of rat mammary carcinoma and its lack of H-ras and Tp53 Mutations. *Int. J. Radiat. Oncol. Biol. Phys.* **69**, 194–203 (2007).

12. R. J. M. Fry, P. Powers-Risius, E. L. Alpen, E. J. Ainsworth, High-LET radiation carcinogenesis. *Radiat. Res.* **104**, S188 (1985).
13. H. Watanabe, T. Ogiu, M. Nishizaki, N. Fujimoto, S. Kido, Y. Ishimura, K. Shiraki, K. Kuramoto, S. Hirata, S. Shoji, O. Katoh, Induction of ovarian tumors by heavy ion irradiation in B6C3F1 mice. *Oncol. Rep.* **5**, 1377–1380 (1998).
14. F. J. Burns, Y. Jin, K. L. Koenig, S. Hosselet, The low carcinogenicity of electron radiation relative to argon ions in rat skin. *Radiat. Res.* **135**, 178–188 (1993).
15. J. F. Dicello, A. Christian, F. A. Cucinotta, D. S. Gridley, R. Kathirithamby, J. Mann, A. R. Markham, M. F. Moyers, G. R. Novak, S. Piantadosi, R. Ricart-Arbona, D. M. Simonson, J. D. Strandberg, M. Vazquez, J. R. Williams, Y. Zhang, H. Zhou, D. Huso, In vivo mammary tumourigenesis in the Sprague–Dawley rat and microdosimetric correlates. *Phys. Med. Biol.* **49**, 3817–3830 (2004).
16. C. J. Shellabarger, J. W. Baum, S. Holtzman, J. P. Stone, Neon-20 ion- and x-ray-induced mammary carcinogenesis in female rats. *Ann. N. Y. Acad. Sci.* **459**, 239–244 (1985).
17. L. C. Solberg Woods, QTL mapping in outbred populations: Successes and challenges. *Physiol. Genomics* **46**, 81–90 (2014).
18. D. M. Gatti, K. L. Svenson, A. Shabalin, L. Y. Wu, W. Valdar, P. Simecek, N. Goodwin, R. Cheng, D. Pomp, A. Palmer, E. J. Chesler, K. W. Broman, G. A. Churchill, Quantitative trait locus mapping methods for diversity outbred mice. *G3* **4**, 1623–1633 (2014).
19. R. Mott, J. Flint, Prospects for complex trait analysis in the mouse. *Mamm. Genome* **19**, 306–308 (2008).
20. W. Valdar, L. C. Solberg, D. Gauguier, S. Burnett, P. Klenerman, W. O. Cookson, M. S. Taylor, J. N. Rawlins, R. Mott, J. Flint, *Nat. Genet.* **38**, 879–887 (2006).
21. K. L. Svenson, D. M. Gatti, W. Valdar, C. E. Welsh, R. Cheng, E. J. Chesler, A. A. Palmer, L. McMillan, G. A. Churchill, High-resolution genetic mapping using the mouse diversity outbred population. *Genetics* **190**, 437–447 (2012).
22. R. Mott, J. Flint, Dissecting quantitative traits in mice. *Annu. Rev. Genomics Hum. Genet.* **14**, 421–439 (2013).
23. K. Demarest, J. McCaughran Jr., E. Mahjubi, L. Cipp, R. Hitzemann, Identification of an acute ethanol response quantitative trait locus on mouse chromosome 2. *J. Neurosci.* **19**, 549–561 (1999).
24. National Research Council Space Studies Board, *Radiation Hazards to Crews of Interplanetary Missions: Biological Issues and Research Strategies* (National Academy Press, 1996).
25. T. Slaba, S. Blattnig, J. Norbury, A. Rusek, C. La Tessa, S. Walker, "GCR simulator reference field and a spectral approach for laboratory simulation" (NASA Technical Paper 2015–218698, 2015).
26. M. M. Weil, F. A. Ray, P. C. Genik, Y. Yu, M. McCarthy, C. M. Fallgren, R. L. Ullrich, Effects of ^{28}Si ions, ^{56}Fe ions, and protons on the induction of murine acute myeloid leukemia and hepatocellular carcinoma. *PLOS ONE* **9**, e104819 (2014).
27. F. A. Cucinotta, Space radiation risks for astronauts on multiple international space station missions. *PLOS ONE* **9**, e96099 (2014).
28. F. A. Cucinotta, M. Y. Kim, L. J. Chappell, Space Radiation Cancer Risk Projections and Uncertainties—2012, Tables A3 and A7, (NASA/TP-2013-217375, 2013).
29. R. Cheng, C. C. Parker, M. Abney, A. A. Palmer, Practical considerations regarding the use of genotype and pedigree data to model relatedness in the context of genome-wide association studies. *G3* **3**, 1861–1867 (2013).
30. R. W. Doerge, G. A. Churchill, Empirical threshold values for quantitative trait mapping. *Genetics* **138**, 963–971 (1994).
31. J. R. Wang, F. P. de Villena, L. McMillan, Comparative analysis and visualization of multiple collinear genomes. *BMC Bioinformatics* **13**, S13 (2012).
32. W. Valdar, C. C. Holmes, R. Mott, J. Flint, Mapping in structured populations by resample model averaging. *Genetics* **182**, 1263–1277 (2009).
33. R. H. Mole, Radiation-induced acute myeloid leukemia in the mouse: Experimental observations in vivo with implications for hypotheses about the basis of carcinogenesis. *Leuk. Res.* **10**, 859–865 (1986).
34. D. L. Preston, S. Kusumi, M. Tomonaga, S. Izumi, E. Ron, A. Kuramoto, N. Kamada, H. Dohy, T. Matsui, H. Nonaka, D. E. Thompson, M. Soda, K. Mabuchi, Cancer incidence in atomic bomb survivors. Part III. Leukemia, lymphoma and multiple myeloma, 1950–1987. *Radiat. Res.* **137**, S68–S97 (1994).
35. R. H. Mole, D. G. Papworth, M. J. Corp, The dose-response for x-ray induction of myeloid leukaemia in male CBA/H mice. *Br. J. Cancer* **47**, 285–291 (1983).
36. R. L. Ullrich, R. J. Preston, Myeloid leukemia in male RFM mice following irradiation with fission spectrum neutrons or γ rays. *Radiat. Res.* **109**, 165–170 (1987).
37. W. D. Cook, B. J. McCaw, C. Herring, D. L. John, S. J. Foote, S. L. Nutt, J. M. Adams, PU.1 is a suppressor of myeloid leukemia, inactivated in mice by gene deletion and mutation of its DNA binding domain. *Blood* **104**, 3437–3444 (2004).
38. P. Y. Chang, F. A. Cucinotta, K. A. Bjornstad, J. Bakke, C. J. Rosen, N. Du, D. G. Fairchild, E. Cacao, E. A. Blakely, Harderian gland tumorigenesis: Low-dose and LET response. *Radiat. Res.* **185**, 449–460 (2016).
39. W. Valdar, L. C. Solberg, D. Gauguier, W. O. Cookson, J. N. Rawlins, R. Mott, J. Flint, Genetic and environmental effects on complex traits in mice. *Genetics* **174**, 959–984 (2006).
40. W. Valdar, J. Flint, R. Mott, Simulating the collaborative cross: Power of quantitative trait loci detection and mapping resolution in large sets of recombinant inbred strains of mice. *Genetics* **172**, 1783–1797 (2005).
41. G. A. Churchill, D. M. Gatti, S. C. Munger, K. L. Svenson, The diversity outbred mouse population. *Mamm. Genome* **23**, 713–718 (2012).
42. M. A. Bogue, G. A. Churchill, E. J. Chesler, Collaborative cross and diversity outbred data resources in the mouse phenome database. *Mamm. Genome* **26**, 511–520 (2015).
43. H. S. Kaplan, M. B. Brown, Further observations on inhibition of lymphoid tumor development by shielding and partial-body irradiation of mice. *J. Natl. Cancer Inst.* **12**, 427–436 (1951).
44. H. S. Kaplan, M. B. Brown, J. Paull, Influence of bone-marrow injections on involution and neoplasia of mouse thymus after systemic irradiation. *J. Natl. Cancer Inst.* **14**, 303–316 (1953).
45. V. C. Martins, K. Busch, D. Juraeva, C. Blum, C. Ludwig, V. Rasche, F. Lasitschka, S. E. Mastitsky, B. Brors, T. Hielscher, H. J. Fehling, H. R. Rodewald, Cell competition is a tumour suppressor mechanism in the thymus. *Nature* **509**, 465–470 (2014).
46. Y. Peng, N. Brown, R. Finnon, C. L. Warner, X. Liu, P. C. Genik, M. A. Callan, F. A. Ray, T. B. Borak, C. Badie, S. D. Bouffler, R. L. Ullrich, J. S. Bedford, M. M. Weil, Radiation leukemogenesis in mice: Loss of PU.1 on chromosome 2 in CBA and C57BL/6 mice after irradiation with 1 GeV/nucleon ^{56}Fe ions, x rays or γ rays. Part I. Experimental observations. *Radiat. Res.* **171**, 474–483 (2009).
47. B. R. Davies, D. S. Finnigan, S. K. Smith, B. A. Ponder, Administration of gonadotropins stimulates proliferation of normal mouse ovarian surface epithelium. *Gynecol. Endocrinol.* **13**, 75–81 (2009).
48. B. C. Vanderhyden, T. J. Shaw, J.-F. Ethier, Animal models of ovarian cancer. *Reprod. Biol. Endocrinol.* **1**, 67 (2003).
49. C. C. Capen, Mechanisms of hormone-mediated carcinogenesis of the ovary. *Toxicol. Pathol.* **32** (Suppl 2), 1–5 (2016).
50. L. Lick, A. Kirschbaum, H. Mixer, Mechanism of induction of ovarian tumors by x-rays. *Cancer Res.* **9**, 532–536 (1949).
51. H. S. Kaplan, Influence of ovarian function on incidence of radiation-induced ovarian tumors in mice. *J. Natl. Cancer Inst.* **11**, 125–132 (1950).
52. B. Mishra, L. Ortiz, U. Luderer, Charged iron particles, components of space radiation, destroy ovarian follicles. *Hum. Reprod.* **31**, 1816–1826 (2016).
53. M. N. Nikiforova, J. R. Stringer, R. Blough, M. Medvedovic, J. A. Fagin, Y. E. Nikiforov, Proximity of chromosomal loci that participate in radiation-induced rearrangements in human cells. *Science* **290**, 138–141 (2000).
54. V. Roukos, T. Misteli, The biogenesis of chromosome translocations. *Nat. Cell Biol.* **16**, 293–300 (2014).
55. D. J. Clark, E. I. Meijne, S. D. Bouffler, R. Huiskamp, C. J. Skidmore, R. Cox, A. R. Silver, Microsatellite analysis of recurrent chromosome 2 deletions in acute myeloid leukaemia induced by radiation in F1 hybrid mice. *Genes Chromosomes Cancer* **16**, 238–246 (1996).
56. F. A. Cucinotta, M. H. Kim, L. J. Chappell, J. L. Huff, How safe is safe enough? Radiation risk for a human mission to Mars. *PLOS ONE* **8**, e74988 (2013).
57. D. Russo, T. Foley, K. Stroud, J. Connolly, B. Tillman, L. Pickett, NASA space flight human system standards. *Proc. Hum. Factors Ergon. Soc. Annu. Meet.* **51**, 1468–1470 (2007).
58. F. A. Cucinotta, L. J. Chappell, M.-H. Kim, M. Wang, Radiation carcinogenesis risk assessments for never-smokers. *Health Phys.* **103**, 643–651 (2012).
59. A. P. Morgan, C.-P. Fu, C.-Y. Kao, C. E. Welsh, J. P. Didion, L. Yadgary, L. Hyacinth, M. T. Ferris, T. A. Bell, D. R. Miller, P. Giusti-Rodriguez, R. J. Nonneman, K. D. Cook, J. K. Whitmire, L. E. Gralinski, M. Keller, A. D. Attie, G. A. Churchill, P. Petkov, P. F. Sullivan, J. R. Brennan, L. McMillan, F. Pardo-Manuel de Villena, The mouse universal genotyping array: From substrains to subspecies. *G3* **6**, 263–279 (2015).
60. H. Morse III, M. R. Anver, T. N. Frederickson, D. C. Haines, A. W. Harris, N. L. Harris, E. S. Jaffe, S. C. Kogan, I. C. MacLennan, P. K. Pattengale, J. Ward; Hematopathology subcommittee of the Mouse Models of Human Cancers Consortium, Bethesda proposals for classification of lymphoid neoplasms in mice. *Blood* **100**, 246–258 (2002).

Acknowledgments: We thank R. Hitzemann (Oregon Health and Sciences University) for providing mice and detailed breeding information. We also thank A. Rusek and the NASA Space Radiation Lab (NSRL) at Brookhaven National Laboratory (BNL). **Funding:** This work was supported by NASA grants NNX12AB54G and NASA NNX15AK13G, and NIH training grant 4T32OD010437-15 (E.F.E.) and R01GM070683 (D.M.G.). Additional funding came from NIH AA13484; NIH R24 AA020245; and NIH U01 AA013519 for the HS/Npt mice. **Author contributions:** E.F.E. and M.M.W. conceived the project and developed the methodology and experiments. E.F.E., E.L.G., C.M.F., and F.A.R. performed investigation, experimentation, provision of study materials, and data collection. E.F.E.

and D.A.K. interpreted mouse histopathology and hematology. E.F.E. and D.M.G. curated SNP data and chromosome reconstructions, created bioinformatics approaches, and interpreted data. E.F.E. created the original draft, and E.F.E., D.M.G., and M.M.W. contributed text to the manuscript. M.M.W. supervised the project, and E.F.E provided project administration. **Competing interests:** The authors declare that they have no competing interests. **Data and material availability:** All data needed to evaluate the conclusions in the paper are present in the paper and/or the Supplementary Materials. Data and code for this project are archived and available at https://github.com/elijahedmondson/NASA-GRSD-HS.

Submitted 5 April 2019
Accepted 14 January 2020
Published 15 April 2020
10.1126/sciadv.aax5940

Citation: E. F. Edmondson, D. M. Gatti, F. A. Ray, E. L. Garcia, C. M. Fallgren, D. A. Kamstock, M. M. Weil, Genomic mapping in outbred mice reveals overlap in genetic susceptibility for HZE ion– and γ-ray–induced tumors. *Sci. Adv.* **6**, eaax5940 (2020).